Journal of Soft Computing Exploration
Homepage: htttps://shmpublisher.com/index.php/joscex
p-ISSN: 2746-7686
e-ISSN: 2746-0991

.

Bio-inspired metaheuristic MPPT algorithms for PV battery systems: a comparative performance study

Faiq Mananul Faqih[1], Rizky Ajie Aprilianto[2]
[1,2]Department of Electrical Engineering, Universitas Negeri Semarang, Indonesia

Article Info

Article history:

Received Mar 12, 2026
Revised Apr 02, 2026
Accepted Apr 02, 2026

Keywords:

Maximum power point tracking
Metaheuristic algorithm
Clean energy
Photovoltaic system
Electric power optimization

ABSTRACT

Maximum Power Point Tracking (MPPT) has been proven to improve power extraction in photovoltaic (PV) systems. However, conventional MPPT methods such as Perturb and Observe (P&O) and Incremental Conductance (InC) have limitations, such as oscillations in steady state conditions, slow response, and a tendency to get stuck at local maxima when irradiation changes. This study aims to evaluate biology-inspired metaheuristic algorithms to improve tracking accuracy, convergence speed, and MPPT stability in PV systems. These algorithms include Grey Wolf Optimization (GWO), Sand Cat Swarm Optimization (SCSO), Horse Herd Optimization (HHO), Chameleon Swarm Algorithm (CSA), and Flying Squirrel Search Optimization (FSSO). The algorithms were tested using the same general parameters to ensure a fair comparison. Testing was conducted on PV models, DC boost converters with resistive loads and batteries under static and dynamic irradiation conditions using MATLAB/Simulink. The results show that HHO provides the best performance with an efficiency of 99.96% at 1000 W/m² and 98.03% at 800 W/m², a tracking time of <0.05 seconds, and power fluctuations of <0.3% in resistive load testing. In battery testing, CSA and FSSO showed the best performance with voltage stability, high charging current, and lower ripple. Overall, the results of this study indicate that the proposed metaheuristic-based MPPT algorithm can improve the accuracy of maximum power point tracking, accelerate convergence time, and minimize power oscillations in PV systems.

Corresponding Author:

Rizky Ajie Aprilianto,
Department of Electrical Engineering,
Universitas Negeri Semarang,
Gunungpati, Semarang City, Central Java, Indonesia 50229.
Email: rizkyajie@mail.unnes.ac.id
https://doi.org/10.52465/joscex.v7i1.13

1. INTRODUCTION

The increasing global demand for energy, coupled with dwindling fossil fuel reserves, has accelerated the transition to renewable energy [1]. Among the various renewable energy technologies available, photovoltaic (PV) solar energy occupies a strategic position due to its scalability, emission-free nature, and low operational and maintenance costs [2]. Global PV installation capacity has continued to experience significant growth over the past decade, reflecting massive adoption in the residential, commercial, and

industrial sectors [3]. Along with this development, low-power PV applications, including wireless sensor systems, IoT devices, portable electronics, and small-scale off-grid systems, are gaining attention as energy supply solutions in both urban and remote areas [4]. These systems generally operate in the range of a few watts to hundreds of watts and require high power extraction efficiency given the limited available power capacity [5].

In maximizing the power harvested from PV modules, Maximum Power Point Tracking (MPPT) is used as a control strategy that continuously operates the PV system at the maximum power point (MPP) even though irradiation and temperature conditions vary [6], [7]. Conventional MPPT methods such as Perturb and Observe (P&O) and Incremental Conductance (INC) have been widely applied due to their simplicity and low computational requirements [8], [9]. However, these methods have several fundamental limitations. Under steady-state conditions, both methods produce oscillations around the MPP, causing power losses and ripple in the system output [10]. Additionally, the response speed to rapid irradiation changes is relatively slow, so the operating point can deviate from the MPP immediately after environmental conditions change [11]. These limitations become more evident under complex operating conditions, such as partial shading in multi-module configurations, where the P–V curve may exhibit multiple local maxima and gradient-based algorithms risk converging to a suboptimal operating point rather than the true MPP [12], [13]. These shortcomings have driven the development of more reliable MPPT methods capable of addressing the characteristics of PV systems under real-world operating conditions, particularly system response time.

In response to the limitations of conventional methods, intelligent optimization algorithms such as bio-inspired metaheuristics have been extensively researched and developed as superior alternatives [14]. Unlike gradient-based methods, metaheuristic algorithms perform stochastic global searches across the entire P–V characteristic surface, thereby avoiding local maxima and finding GMPP [15]. These algorithms mimic collective behavior and natural phenomena found in biological systems, such as animal hunting strategies, insect foraging behavior, and animal herd movement patterns [16]. Population-based search mechanisms enable simultaneous exploration of many candidate solutions, resulting in high robustness and adaptability to highly nonlinear and multimodal optimization landscapes [17]. When applied to MPPT systems, this algorithm generates a duty cycle reference for DC-DC converters according to the operating voltage at the GMPP, making it particularly suitable for systems facing dynamic environmental conditions [18].

Various metaheuristic algorithms have been reported in literature as MPPT methods with better performance than conventional methods. The Grey Wolf Optimizer (GWO), which mimics the hierarchical leadership behavior and cooperative hunting strategies of gray wolves, has been applied to PV systems and has demonstrated fast convergence and high MPP tracking accuracy [19]. Sand Cat Swarm Optimization (SCSO), inspired by the nocturnal hunting behavior of sand cats, has been proposed as an alternative with fewer parameters but still has competitive global search capabilities [20]. Horse Herd Optimization Algorithm (HHO), which mimics the social dynamics and movement of horse herds, shows a good balance of exploration and exploitation in various engineering optimization problems [21]. Meanwhile, Flying Squirrel Search Optimization (FSSO), which mimics the gliding and foraging behavior of flying squirrels, has been reported to achieve competitive performance in multimodal optimization scenarios [22]. However, most existing studies evaluate these algorithms exclusively using fixed and ideal resistive loads. The behavior of these algorithms when faced with dynamic and nonlinear battery loads has not yet been studied.

This study presents an evaluation and comparison of the performance of bio-inspired metaheuristic MPPT algorithms, including GWO, SCSO, HHO, Chameleon Swarm Algorithm (CSA), and FSSO, implemented in a low-power PV system using a DC boost converter. These algorithms were selected based on their foraging behavior, which inherently reflects the process of determining an optimal point within a complex search space like determining the MPP on a nonlinear P–V curve. A battery load was used to provide more realistic and dynamically varying characteristics. Each algorithm was implemented and tested under standard testing conditions (STC) and under irradiation variation scenarios using MATLAB/Simulink simulations. The performance metrics analyzed included tracking efficiency, tracking time, and power ripple. The results obtained are expected to provide a comprehensive basis for assessing the suitability of each algorithm for PV-based battery charging applications, as well as practical guidance in selecting MPPT algorithms for low-power off-grid PV systems.

2. METHOD

PV Module Modelling

The low-power PV system used in this study is shown in Figure 1. This system consists of a PV module, a metaheuristic algorithm-based MPPT controller, and a DC–DC boost converter connected to a battery load. Radiation intensity ($Irra$) and ambient temperature (T) are used as inputs to generate PV voltage (V_{pv}) and current (I_{pv}). These values are then processed to determine the optimal duty cycle (D) as a pulse width modulation (PWM) signal for the converter, so that the system always operates at the maximum power

point (MPP). Mathematical modeling of the PV module uses a single diode equivalent circuit approach, consisting of photon current (I_{ph}), an ideal diode with saturation current (I_s), series resistance (R_s), and parallel resistance (R_{sh}). The current-voltage relationship is expressed by (1) [8].

$$I = I_{ph} - I_s\left(e^{\frac{q(V+IR_s)}{nkT}} - 1\right) - \frac{V + IR_s}{R_{sh}} \quad (1)$$

where q is the electron charge, n is the diode ideality factor, k is the Boltzmann constant, and T is the absolute temperature of the cell. The PV output power is obtained from (2).

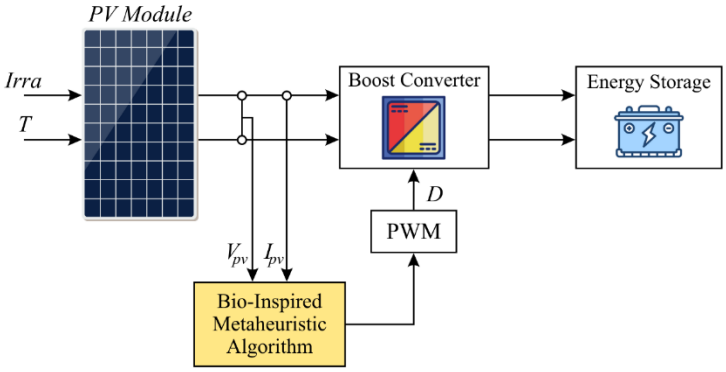

Figure 1. MPPT photovoltaic system framework

$$P = V \times I \quad (2)$$

The photon current I_{ph} depends on the irradiance (G) and temperature (T) based on (3).

$$I_{ph} = [I_{sc,ref} + K_i(T - T_{ref})]\frac{G}{G_{ref}} \quad (3)$$

where $I_{sc,ref}$ is the reference short-circuit current, K_i is the current temperature is coefficient, and G_{ref} and T_{ref} are the reference irradiance and temperature, respectively. These equations are used to determine the $I - V$ and $P - V$ characteristics of PV modules under various irradiance levels.

The PV module used is the BISOL BMO-250 W, the main parameters presented in Table 1.

Table 1. Specifications of BISOL BMO-250 W

Parameter	Description	Value
P_{max}	Maximum Power	250.10 W
V_{mp}	Voltage at MPP	30.5 V
I_{mp}	Current at MPP	8.20 A
V_{oc}	Open Circuit Voltage	37.9 V
I_{sc}	Short Circuit Current	8.80 A

Boost Converter

A boost-type DC-DC converter increases the output voltage from the PV module to match the battery load requirements. Its working principle is based on the storage and release of energy through an inductor, which is controlled by a PWM signal with a specific duty cycle (D) [23]v. When the power switch is ON, current flows from the PV source to the inductor, storing energy in the form of a magnetic field. Conversely, when the switch is OFF, the energy stored in the inductor is released to the load through a diode, causing the output voltage to increase beyond the input voltage ($V_o > V_{in}$). The relationship between the input voltage and the output voltage under ideal conditions is expressed as follows (4).

$$V_o = \frac{V_{in}}{1 - D} \quad (4)$$

where D is the ratio of the switch ON time to the total switching period. The greater the value of D, the higher the output voltage produced by the converter.

To ensure stable converter performance, the design of passive components, such as inductors (L) and capacitors (C) must consider the allowable ripple current and ripple voltage. The inductor value is calculated using (5) [24]. Meanwhile, the capacitor value is determined using (6).

$$L = \frac{V_{in} \times D}{\Delta I_L \times f_s} \quad (5)$$

$$C = \frac{I_o \times D}{\Delta V_o \times f_s} \quad (6)$$

where V_{in} is the input voltage of the PV, I_o is the output current, ΔI_L is the inductor ripple current, ΔV_o is the output ripple voltage, and f_s is the sampling frequency.

These parameters are optimized to ensure the converter operates in Continuous Conduction Mode (CCM), where the inductor current remains nonzero throughout the switching cycle. Table 2 presents the main parameters of the boost converter used in this simulation.

Table 2. Parameter of boost converter

Parameter	Value	Unit
Maximum power rating (P_{max})	250	W
Switching frequency (f_{sw})	30	kHz
Input voltage (V_{in})	20 - 40	V
Input current (I_{in})	13.2	A
Output voltage (V_{out})	76	V
Output current (I_{out})	3.29	A
Inductor (L)	1.3	mH
Input capacitor (C_{in})	1000	µF
Output capacitor (C_{out})	440	µF
Switching frequency (f_s)	30	kHz

Battery Parameter

The battery used in this simulation is modeled using a Lead-Acid battery block. Lead-Acid batteries are commonly used in low-power off-grid PV systems due to their reliability and wide availability [25]. The battery model parameters used in this study are summarized in Table 3.

Table 3. Battery parameters

Parameter	Value	Unit
Battery type	Lead-Acid	-
Nominal voltage	72	V
Rated capacity	20	Ah
Internal resistance	0.036	Ω
Cut off voltage	54	V

The MATLAB/Simulink Lead-Acid battery model implements the Shepherd curve-fitting method, which characterizes the nonlinear relationship between terminal voltage and state of charge (SoC). Unlike an ideal resistive load where terminal voltage adjusts freely and proportionally to current, the Lead-Acid battery terminal voltage is governed by its electrochemical SoC, exhibiting a nonlinear and time-varying impedance characteristic. As the battery charges, its terminal voltage gradually rises while internal resistance varies with SoC, continuously shifting the PV operating point away from the MPP.

Bio Inspired Metaheuristic MPPT Algorithms

Grey wolf optimization

GWO is a metaheuristic algorithm introduced by Mirjalili in 2014 [26], inspired by the hierarchical hunting behavior of grey wolf (Canis lupus) packs, which are structured into four ranks: *α, β, δ* as leaders and *ω* as followers. In MPPT application, the three best duty cycle candidates are assigned as *α, β,* and *δ*, while the remaining agents iteratively update their positions guided by these leaders. The distance between each agent and the optimal solution is computed using (7), and the position update follows (8).

$$D = \left| C \cdot X_p(t) - X(t) \right| \quad (7)$$

$$X(t+1) = X_p(t) - A \cdot D \quad (8)$$

The coefficients $A = 2a \cdot r_1 - a, C = 2r_2$ regulate the exploration–exploitation balance, where parameter *a* decrease linearly from 2 to 0 over iterations, and r_1, $r_2 \in [0,1]$ are random values. The final position is computed as the average influence of *α*, *β*, and *δ*, with the fitness function defined as the instantaneous PV output power, as given by (9).

$$Fitness = P = V_{pv} \times I_{pv} \quad (9)$$

Sand cat swarm optimization

SCSO is a metaheuristic algorithm that mimics the prey-detection behavior of sand cats through low-frequency sound sensitivity [27]. The algorithm controls the exploration–exploitation transition via an adaptive sensitivity parameter r_G, which decreases linearly from its maximum value SM to zero as iterations progress (10), with the actual agent sensitivity computed stochastically as $r = r_G \times rand$. A balancing parameter $R = 2r_G \times rand - r_G$ determines the search mode: $|R| > 1$ triggers exploration, while $|R| \leq 1$ triggers exploitation.

$$r_G = SM\left(1 - \frac{n}{n_{max}}\right) \tag{10}$$

During exploration, agents perform random searches around the current best position (11). During exploitation, the position update incorporates a cosine-based directional movement toward the global optimum (12), where the angle θ is selected via roulette wheel to ensure smooth local convergence.

$$d^{n+1} = r \cdot (d_{bc}(n) - rand \cdot d_c(n)) \tag{11}$$

$$d^{n+1} = d_b(n) - r \cdot d_{rnd} \cdot \cos(\theta) \tag{12}$$

The fitness function is defined as $f(d) = P_{pv}(d) = V_{pv}(d) \cdot V_{pv}(d)$, and the algorithm restarts when irradiance change exceeds 5% to prevent entrapment at a local MPP.

Horse herd optimization

HHO is a metaheuristic algorithm inspired by the collective social behavior of horse herds vv [28], where each agent (horse) is characterized by a position *X* representing the duty cycle candidate and a velocity *V* governing its movement direction. Horses are categorized into four age groups α (>15 year), β (10-15 year), γ (5-10 year), and δ (0-5 year) each exhibiting different combinations of six behavioral mechanisms: grazing (G), hierarchy (H), sociability (S), imitation (I), defense (D), and roaming (R). The velocity per age group is computed as follows (12), and the position is updated via (11).

$$X_m^{Iter,AGE} = V_m^{Iter,AGE} + X_m^{(Iter-1),AGE}, \qquad AGE = \alpha, \beta, \gamma, \delta \tag{11}$$

$$\begin{aligned} V_m^{Iter,\alpha} &= G_m^{Iter,\alpha} + D_m^{Iter,\alpha} \\ V_m^{Iter,\beta} &= G_m^{Iter,\beta} + H_m^{Iter,\beta} + S_m^{Iter,\beta} + D_m^{Iter,\beta} \\ V_m^{Iter,\gamma} &= G_m^{Iter,\gamma} + H_m^{Iter,\gamma} + S_m^{Iter,\gamma} + I_m^{Iter,\gamma} + D_m^{Iter,\gamma} + R_m^{Iter,\gamma} \\ V_m^{Iter,\delta} &= G_m^{Iter,\delta} + I_m^{Iter,\delta} + R_m^{Iter,\delta} \end{aligned} \tag{12}$$

Among the six mechanisms, grazing drives initial exploration across the duty cycle space; hierarchy and sociability direct horses toward the best and mean herd positions, respectively; imitation attracts young horses toward the top-performing agents; defense repels agents from low-fitness regions; and roaming introduces random perturbation to escape local optima. Each behavioral coefficient decreases progressively through a reduction factor w per iteration, enabling a gradual transition from global exploration to local exploitation. The fitness function is defined as $P = V_{pv} \times I_{pv}$, and the horse position with the highest fitness at termination is selected as the optimal duty cycle.

Flying squirrel search optimization

FSSO analogizes PV output power as a food source, with the duty cycle as the decision variable representing each agent's position [29]. Agents are classified into three roles based on fitness ranking: the best solution occupies the hickory tree, the second-best the acorn tree, and the remaining agents occupy normal trees as explorers. Position updates are governed by two mechanisms operating in parallel.

The first is seasonal monitoring, which evaluates the distance between the acorn and hickory tree positions to determine the exploitation rate (13).

$$\begin{aligned} S_C^k &= | d_{\text{aco-tree}}^k - d_{\text{hick-tree}}^k |; \ \text{if } S_C^k < S_{\min} \\ S_{min} &= \frac{10^{-6}}{365^{2.5k/k_m}}; \ otherwise \end{aligned} \tag{13}$$

When the seasonal constant S_C falls below threshold S_{min}, agents glide directly toward the hickory tree using (14-16), where G is the gliding constant and g_d is the gliding distance derived from the aerodynamic ratio $\frac{C_D}{C_L}$ of flying squirrels.

$$d_{\text{aco-tree}}^{k+1} = d_{\text{aco-tree}}^{k} + G\, g_d(d_{\text{hick-tree}}^{k} - d_{\text{aco-tree}}^{k}) \quad (14)$$

$$d_{\text{norm-tree}}^{k+1} = d_{\text{norm-tree}}^{k} + G\, g_d(d_{\text{hick-tree}}^{k} - d_{\text{norm-tree}}^{k}) \quad (15)$$

$$d_{\text{norm-tree}}^{k+1} = d_{\text{norm-tree}}^{k} + G\, g_d(d_{\text{aco-tree}}^{k} - d_{\text{norm-tree}}^{k}) \quad (16)$$

The second is Lévy flight, applied when $S_C \geq S_{min}$ to enhance exploration and prevent entrapment at local optima. The step length incorporates a gamma function with Lévy index β = 1.5, producing heavy-tailed random jumps that increase search diversity. The algorithm is reinitialized when a significant change in PV power is detected, indicating an irradiance shift, ensuring adaptive re-tracking of the new GMPP.

Chameleon swarm agorithm

CSA is a metaheuristic algorithm inspired by the dynamic hunting behavior of chameleons, encompassing three biological mechanisms: prey searching (eye movement), local search (eye rotation), and exploitation (tongue projection) [30]. In MPPT, each agent represents a duty cycle candidate initialized randomly within $[D_{min}, D_{max}]$.

During prey searching, the position of each chameleon is updated based on its personal best ($P_{best,i}$) and the global best (G_{best}) calculated as (17). When $r\_r_i \geq P_p$, the agent moves toward both attractors; otherwise, a random perturbation scaled by adaptive parameter μ is applied to maintain search diversity.

$$D_i^{t+1} = \begin{cases} D_i^t + p_1\left(P_{best,i} - D_i^t\right)r_2 + p_2(G_{best} - D_i^t)r_1, & \text{if } r_i \geq P_p \\ D_i^t + \mu\left((D_{max} - D_{min})r_3 + D_{min}\right) \cdot sgn(rand - 0.5), & \text{if } r_i < P_p \end{cases} \quad (17)$$

During local search, a rotation matrix m is applied to simulate the independent rotation of the chameleon's eyes, refining the search around the current position. In the exploitation phase, when the agent is close to the MPP, tongue projection is modeled through a velocity update governed by inertia weight ω and acceleration coefficients c_1, c_2, followed by a position update using tongue acceleration a = 2590 m/s². The fitness function is defined as $P = V_{pv} \times I_{pv}$, and the agent position corresponding to the highest power is selected as the optimal duty cycle.

Testing Scenarios

The performance evaluation of the MPPT algorithm is based on two test scenarios using uniform parameter configurations as shown in Table 4. The first scenario is STC conditions (1000 W/m², 25°C) to assess tracking accuracy and stability under steady-state conditions, while the second scenario is dynamic conditions with gradual variations in light intensity from 600 to 1000 W/m² to evaluate the algorithm's response to changes in environmental conditions. The test scenario is designed based on a single 250-W PV module configuration. In this configuration, partial shading conditions where solar radiation intensity is spatially uneven across multiple modules simultaneously do not apply. Therefore, the radiation intensity scenario presented represents uniform temporal variations, which constitute a relevant MPPT challenge for single-module systems.

Table 4. General parameters of algorithm testing

Parameter	Value
Duty cycle range	0.1 – 0.59
Max iteration	50
N population	10

The evaluation metrics used in this study include tracking efficiency, convergence time, and power ripples. Tracking efficiency (η_{MPPT}) is used to assess the accuracy of the algorithm in tracking MPP. This value is obtained by comparing the power output generated by the algorithm with the ideal maximum power of the PV, as calculated using (18).

$$\eta_{MPPT} = \frac{P_{MPPT}}{P_{MPP,ideal}} \times 100\% \quad (18)$$

where P_{MPPT} is the power obtained from the algorithm and $P_{MPP,ideal}$ is the ideal maximum power of the PV module.

The convergence time metric is the time required for the algorithm to reach the MPP from the start of the simulation process or after a change in irradiance. Furthermore, the power ripple (ΔP) is used to describe the power fluctuations in the steady state after the algorithm reaches the MPP obtained using (19). A smaller ΔP value indicates good stability, and vice versa.

$$\Delta P = \frac{P_{max,ss} - P_{min,ss}}{P_{MPP,ideal}} \times 100\% \quad (19)$$

where $P_{max,ss}$ and $P_{min,ss}$ These are the maximum and minimum power, respectively, at steady state.

3. RESULTS AND DISCUSSIONS

Initial testing was conducted using resistive loads to evaluate the performance of the MPPT algorithm without the influence of battery nonlinear characteristics. Testing was performed under STC conditions and irradiation variations. The PV voltage response under STC conditions is shown in Figure 2(a). All algorithms quickly increased the voltage from the initial condition to the MPP area, reaching approximately 30.5V, with different transient characteristics. CSA produced the highest steady-state voltage (≈31V) but was accompanied by greater initial oscillations. In contrast, FSSO showed the largest oscillations due to its aggressive initial exploration mechanism, followed by SCSO with smaller fluctuations. HHO and GWO showed the smallest voltage ripples. Additionally, Figure 2(b) shows the PV current response, where all algorithms tend to stabilize the current around the optimal value of 8.2A, with HHO and GWO reaching this value with nearly identical fluctuations, while FSSO and SCSO show larger fluctuations, and CSA produces the lowest current (≈7.95A) with relatively high initial oscillations.

Meanwhile, based on power extraction under STC conditions as shown in Figure 2(c), all algorithms demonstrate the ability to achieve power up to MPP (250.10W). In the initial phase (<0.1 seconds), all algorithms experience oscillations due to duty cycle adjustments. HHO and GWO produce power closest to the ideal MPP of 250.10W, with a steady state value of around 250W and a very small power ripple of 0.08%. The time required to reach MPP for the HHO and GWO algorithms is 0.046 seconds and 0.04 seconds, respectively. SCSO and FSSO successfully reached MPP at 0.074 and 0.081 seconds, respectively, with a power of 248.7W. FSSO produced the largest oscillation among the algorithms, at 0.88%, which is still very good, as <1% is considered excellent tracking stability. CSA produced a power of 248.4W in 0.27 seconds, and this algorithm produced 0.60% less oscillation than FSSO. Furthermore, three periodic noise points are observed at approximately 0.13seconds, 0.27 seconds, and 0.53 seconds across all algorithms, attributed to the periodic global search re-initialization mechanism embedded in each metaheuristic algorithm. These transient disturbances do not affect the steady-state tracking performance, as all algorithms immediately return to the MPP following each re-initialization event. A complete comparison of the algorithms is presented in Table 5.

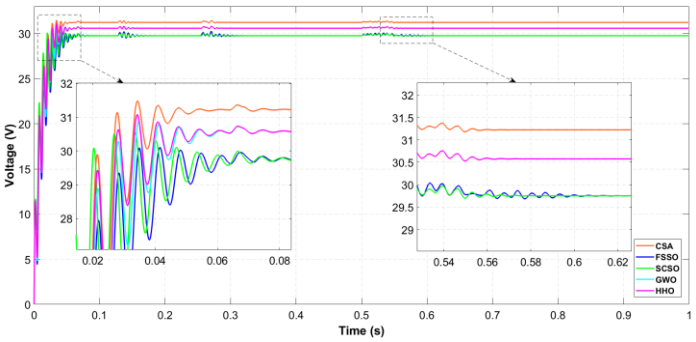

(a)

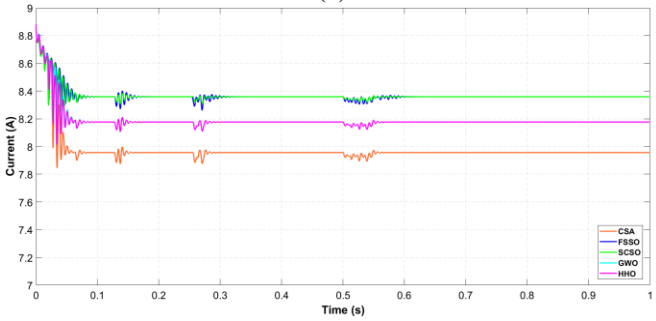

(b)

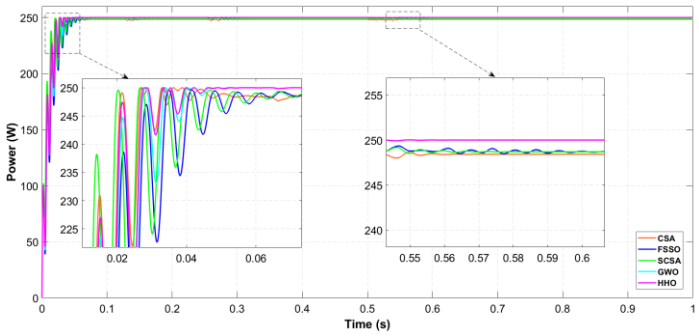

(c)

Figure 2. Algorithm performance under STC (1000 W/m^2, 25°C), (a) Voltage, (b) Current, (c) Power

Table 5. Comparison of STC condition algorithm performance

No	Algorithm	Pmax (W)	Tracking time (s)	ΔP (%)	Power (W)
1	HHO		0.046	0.08	250.00
2	GWO		0.047	0.08	250.00
3	SCSO	250.10	0.074	0.56	248.70
4	FSSO		0.081	0.88	248.70
5	CSA		0.051	0.60	248.40

The response of each algorithm in the irradiation intensity variation scenario, from 1000-800-600W/m², was evaluated to assess its ability to adapt to dynamic environmental conditions, as shown in Figure 3. When the irradiation intensity decreased from 1000 to 800W/m² in the initial phase, the PV output power decreased proportionally. The HHO algorithm achieved the highest power of 198.60W at a voltage of 29.20V, followed by FSSO with a power of 198.50W at an irradiation of 800 W/m², as shown in Figure 3(a). Although the voltage generated by the GWO algorithm oscillates slightly, with smoother current characteristics, the output power oscillation is more stable compared to SCSO. In the CSA algorithm, there is a fluctuation of 1.38%, which is the largest compared to other algorithms.

When the irradiation intensity decreased to 600W/m², the HHO algorithm reached a peak power of 150.6W in 0.02 seconds. The GWO and SCSO algorithms produced similar powers of around 147W, with stabilization times of 0.022 seconds and 0.026 seconds, respectively. The current generated by each algorithm tends to be the same, around 5.10A, as shown in Figure 3(b). However, the voltage values generated vary slightly, causing corresponding power variations. The CSA and FSSO algorithms show slightly large oscillations, 2.22% and 1.89%, at the beginning of the radiation intensity change. The GWO algorithm produces the lowest power at this radiation intensity.

When the radiation intensity rises again to approximately 1000 W/m² at t ≈ 0.83 s, a more pronounced transient oscillation is observed compared to the intensity decay transition. This asymmetric behavior is physically caused by the nonlinear response of the PV module under increasing radiation, where the short-circuit current increases proportionally while the open-circuit voltage rises only logarithmically. This results in a sudden upward shift in the MPP, forcing any algorithm to reinitialize its search across a broader operating region. Furthermore, the battery terminal voltage, limited by its SoC, cannot respond instantly to sudden current surges from the panels. This creates a transient impedance mismatch manifested as voltage undershoot and power overshoot, observable in Figures 3(a) and 3(c). Among these algorithms, HHO and FSSO exhibit the most pronounced power spikes due to their more aggressive exploration mechanisms, whereas CSA, GWO, and SCSO demonstrate relatively smoother convergence. Nevertheless, all algorithms successfully converged to the MPP of approximately 250 W within a fraction of a second, as confirmed in Figure 3(c), with detailed performance metrics summarized in Table 6.

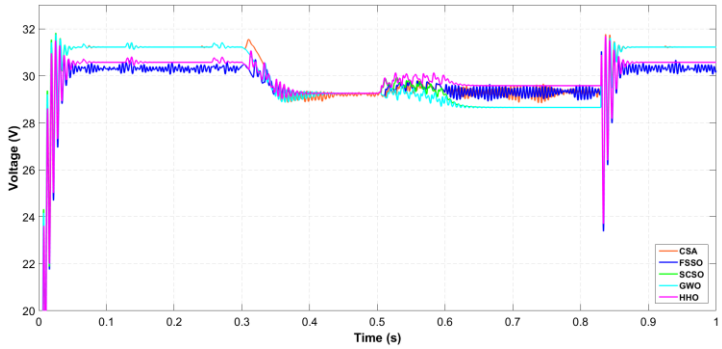

(a)

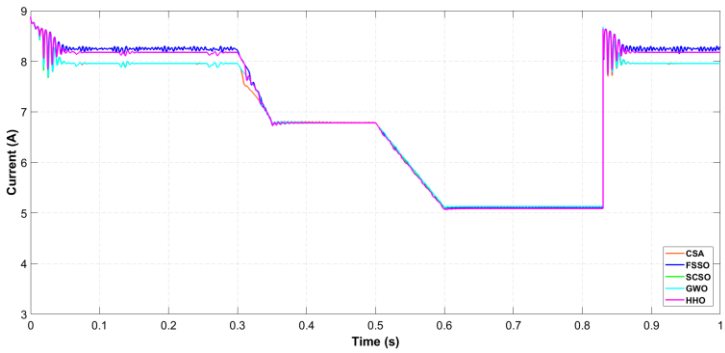

(b)

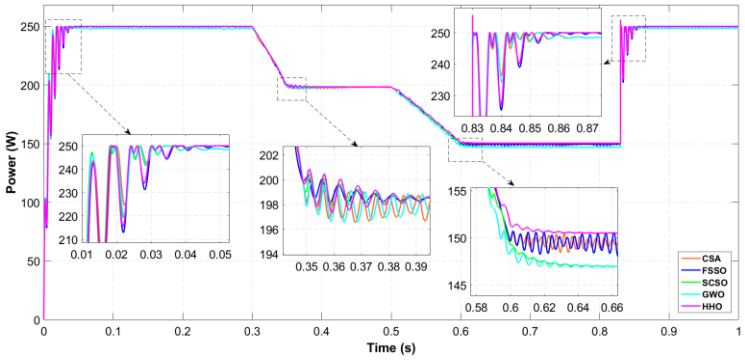

(c)

Figure 3. Algorithm performance under variance irradiance,
(a) Voltage, (b) Current, (c) Power

Table 6. Performance of the MPPT metaheuristic algorithm under varying irradiation conditions

No	Irradiation (W/m^2)	Algorithm	Pmax (W)	Tracking time (s)	ΔP (%)	Power (W)
1	1000	HHO	250.10	0.046	0.08	250.00
		GWO		0.047	0.08	250.00
		SCSO		0.074	0.56	248.70
		FSSO		0.081	0.88	248.70
		CSA		0.051	0.60	248.40
2	800	HHO	202.60	0.032	0.25	198.60
		GWO		0.049	0.69	198.20
		SCSO		0.033	0.84	198.40
		FSSO		0.041	0.35	198.50
		CSA		0.071	1.38	198.00
3	600	HHO	153.50	0.020	0.26	150.60
		GWO		0.022	0.46	147.00
		SCSO		0.026	0.85	147.00
		FSSO		0.034	1.89	149.50
		CSA		0.021	2.22	149.50

Based on the battery voltage graph in Figure 4(a), all algorithms show similar charging characteristics, namely the voltage gradually increases from around 71.75V to ±72.5V. In steady-state conditions, the CSA, FSSO, GWO, and HHO algorithms produce almost identical voltages that are relatively higher than SCSO. A

more obvious difference can be seen in the inset display in the early simulation time range, where SCSO shows transient oscillations with the largest amplitude, while CSA and FSSO show smaller and faster damped oscillations, indicating a more stable transient response. In the battery current graph in Figure 4(b), the initial current surge occurs due to the voltage difference between the converter output and the voltage of the battery terminals that are not yet fully charged. After the transient phase, CSA, FSSO, GWO, and HHO successfully stabilized the charging current at a value of around 3.85–3.9A, while SCSO was only able to reach 2.5–2.7A accompanied by continuous ripple, indicating the inability of SCSO to optimally track the maximum power point when connected to a battery load.

The SoC graph in Figure 4(c) shows a consistent increase across all algorithms, from around 54.955% to nearly 54.958%. Although the change in SoC is relatively small, within a range of ±0.003%, this is normal considering the relatively short simulation duration. The differences between the algorithms are more clearly visible in the inset display around 0.6 seconds, where CSA, GWO, and HHO show the highest SoC values, indicating a faster charging rate, while FSSO is slightly below the other three. The SCSO algorithm again shows the lowest performance with the smallest SoC value, consistent with the lower charging current results as shown in the previous graph.

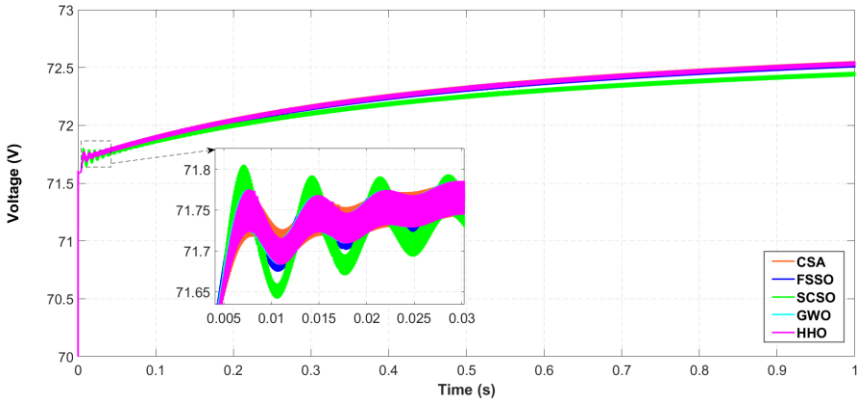

(a)

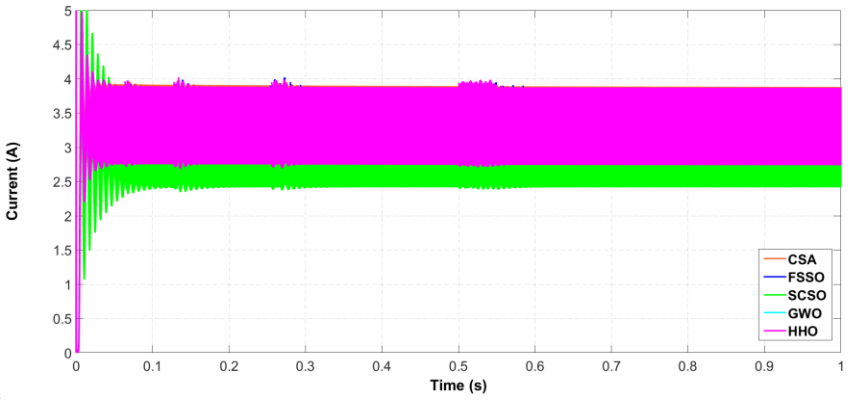

(b)

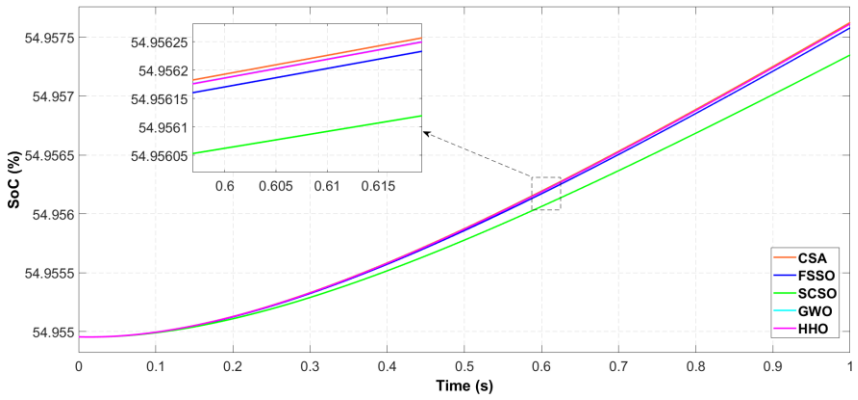

(c)

Figure 4. Battery charging performance using boost converter,
(a) Voltage, (b) Current, (c) SoC

MPPT efficiency was evaluated at three irradiance levels (600, 800, and 1000 W/m²) to assess each algorithm's tracking consistency, with a complete summary of extracted power and efficiency values presented in Table 6. At low irradiance (600 W/m²), HHO achieved the highest efficiency at over 98%, while GWO, SCSO, FSSO, and CSA fell slightly below this value. At medium irradiance (800 W/m²), all algorithms converged to relatively similar efficiency with only marginal differences in extracted power. Under STC conditions (1000 W/m²), nearly all algorithms approached 100% efficiency, reducing inter-algorithm differences to a level primarily governed by each method's convergence precision.

Table 7. MPPT efficiency under different sunlight conditions

Irradiation (W/m^2)		600	800	1000
	Pmax (W)	153.50	202.60	250.10
HHO	Extracted Power (W)	150.60	198.60	250.00
	Efficiency (%)	98.13	98.03	99.96
GWO	Extracted Power (W)	147.00	198.20	250.00
	Efficiency (%)	95.78	97.84	99.96
SCSO	Extracted Power (W)	147.00	198.40	248.70
	Efficiency (%)	95.78	97.93	99.44
FSSO	Extracted Power (W)	149.50	198.50	248.70
	Efficiency (%)	97.41	97.98	99.44
CSA	Extracted Power (W)	149.50	198.00	248.4
	Efficiency (%)	97.41	97.74	99.32

4. CONCLUSION

This study numerically evaluates five metaheuristic algorithms, namely HHO, GWO, CSA, SCSO, and FSSO, for MPPT application in PV systems. Each algorithm is tested on resistive loads and batteries, with the system consisting of one PV module and a DC boost converter. In resistive load testing, all five algorithms analyzed provided satisfactory MPP tracking, with some, such as CSA and FSSO, exhibiting oscillations at the onset of light intensity changes. The GWO and SCSO algorithms experienced a decrease in efficiency under low irradiation conditions. Meanwhile, the HHO algorithm consistently achieved the best performance and highest efficiency under various conditions. Under battery load conditions, CSA and FSSO showed the best performance in terms of voltage stability, high charging current, and lower ripple, followed by GWO and HHO, which continued to perform well, while SCSO produced the lowest performance. Overall, this study makes a significant contribution to the selection of efficient and adaptive MPPT algorithms, reinforcing the potential of metaheuristic methods in the development of solar energy systems.

CREDIT AUTHORSHIP CONTRIBUTION STATEMENT

Faiq Mananul Faqih: Data curation, Formal analysis, Investigation, Methodology, Software, Validation, Visualization. **Rizky Ajie Aprilianto:** Conceptualization, Formal analysis, Investigation, Methodology, Supervision, Writing – original draft, Writing – review and editing.

DECLARATION OF COMPETING INTERESTS

The authors declare no conflicts of interest associated with this paper.

DATA AVAILABILITY

Data will be made available on request.

REFERENCES

[1] J. L. Holechek, H. M. E. Geli, dan M. N. Sawalhah, "A Global Assessment : Can Renewable Energy Replace Fossil Fuels by 2050 ?," *Sustainability*, vol. 14, no. 4792, hal. 1–22, 2022, doi: https://doi.org/10.3390/su14084792.

[2] A. M. Soomar, A. Hakeem, M. Messaoudi, P. Musznicki, A. Iqbal, dan S. Czapp, "Solar Photovoltaic Energy Optimization and Challenges," *Front. Energy Res.*, vol. 10, no. May, hal. 1–18, 2022, doi: 10.3389/fenrg.2022.879985.

[3] I.-I. E. Agency, "Renewables 2025," *www.iea.org*, 2025. .

[4] F. F. Ahmad, C. Ghenai, dan M. Bettayeb, "Maximum power point tracking and photovoltaic energy harvesting for Internet of Things: A comprehensive review," *Sustain. Energy Technol. Assessments*, vol. 47, 2021, doi: 10.1016/j.seta.2021.101430.

[5] O. Lopez-Lapena, M. T. Penella, dan M. Gasulla, "A New MPPT Method for Low-Power Solar Energy Harvesting," *IEEE Trans. Ind. Electron.*, vol. 57, no. 9, hal. 3129–3138, 2010, doi: 10.1109/TIE.2009.2037653.

[6] M. L. Katche, A. B. Makokha, S. O. Zachary, dan M. S. Adaramola, "A Comprehensive Review of Maximum Power Point Tracking (MPPT) Techniques Used in Solar PV Systems," *energies*, vol. 16, no. 2206, 2023, doi:

https://doi.org/10.3390/en16052206.
[7] L. Guanghua, A. Muhammad, S. Hadi, H. Shah, S. Shaikh, dan P. Musznicki, "Results in Engineering Maximum power point tracking strategies for solar PV systems : A review of current methods and future innovations," *Results Eng.*, vol. 28, no. September, hal. 107227, 2025, doi: 10.1016/j.rineng.2025.107227.
[8] R. A. Aprilianto, M. N. Syah, dan A. Suryanto, "A Novel High Gain Modified SEPIC Converter Application for PV Systems," *Int. Conf. Technol. Policy Energy Electr. Power*, 2024, doi: 10.1109/ICT-PEP63827.2024.10733484.
[9] A. Harrison, E. M. Nfah, J. De Dieu, N. Ndongmo, dan N. H. Alombah, "An Enhanced P & O MPPT Algorithm for PV Systems with Fast Dynamic and Steady-State Response under Real Irradiance and Temperature Conditions," *Int. J. Photoenergy*, vol. 2022, 2022, doi: 10.1155/2022/6009632.
[10] M. S. Endiz dan G. Gökku, "A Review of Traditional and Advanced MPPT Approaches for PV Systems Under Uniformly Insolation and Partially Shaded Conditions," *Appl. Sci.*, vol. 15, no. 1031, 2025, doi: https://doi.org/10.3390/ app15031031.
[11] F. Gao, Z. Lin, L. Yin, dan Q. Gao, "Flexible power point tracking for photovoltaic systems based on the linear jump method," *Energy Convers. Manag.*, vol. 333, no. 119805, 2025, doi: https://doi.org/10.1016/j.enconman.2025.119805.
[12] O. F. Tozlu dan O. F. Tozlu, "A Review and Classification of Most Used MPPT Algorithms for Photovoltaic Systems," *Hittite J. Sci. Eng.*, vol. 8, no. 3, hal. 207–220, 2021, doi: 10.17350/HJSE19030000231.
[13] M. Y. Worku, M. A. Hassan, dan L. S. Maraaba, "A Comprehensive Review of Recent Maximum Power Point Tracking Techniques for Photovoltaic Systems under Partial Shading," *Sustainability*, vol. 15, no. 11132, 2023, doi: https://doi.org/10.3390/ su151411132.
[14] R. Nasr dan B. A. Essam, "Metaheuristic Optimization Algorithm-Based Enhancement of Photovoltaic Energy System Performance," *Arab. J. Sci. Eng.*, 2023, doi: 10.1007/s13369-023-07847-0.
[15] H. Eftekhari, A. S. M. Al-obaidi, dan S. Eftekhari, "Aerodynamic Performance of Vertical and Horizontal Axis Wind Turbines : A Comparison Review," *Indones. J. Sci. Technol.*, vol. 7, no. 1, hal. 65–88, 2022.
[16] I. F. Tepe, "Review and Comparative Analysis of Metaheuristic MPPT Algorithms in PV Systems Under Partial Shading Conditions," *IEEE Int. Conf. Renew. Energy Res. Appl.*, hal. 471–479, 2022, doi: 10.1109/ICRERA55966.2022.9922868.
[17] X. Yang dan L. Press, *Nature-Inspired Metaheuristic Algorithms Second Edition*. 2010.
[18] M. Yaich, Y. Dhieb, M. Bouzguenda, dan M. Ghariani, "Metaheuristic Optimization Algorithm of MPPT Controller for PV system application," *E3S Web Conf.*, vol. 336, no. 7, 2022, doi: 10.1051/e3sconf/202233600036.
[19] L. Guanghua *et al.*, "Results in Engineering Comparative analysis of GWO MPPT with conventional techniques in shaded PV arrays," *Results Eng.*, vol. 27, no. August, hal. 106881, 2025, doi: 10.1016/j.rineng.2025.106881.
[20] L. Li, W. Zhao, H. Wang, Z. Xu, dan Y. Ding, "Sand cat swarm optimization based maximum power point tracking technique for photovoltaic system under partial shading conditions," *Int. J. Electr. Power Energy Syst.*, vol. 161, no. March, hal. 110203, 2024, doi: 10.1016/j.ijepes.2024.110203.
[21] M. Agdam *et al.*, "A novel algorithm MPPT controller based on the herd horse optimization for photovoltaic systems under partial shadow conditions," *Eng. Res. Express*, vol. 6, no. 3, 2024, doi: 10.1088/2631-8695/ad5f16.
[22] D. Kumar, R. Dutta, dan D. K. Tanti, "Performance Analysis of Flying Squirrel Search Optimization Technique for MPPT in Photovoltaic System," *Odisha Int. Conf. Electr. Power Eng. Commun. Comput. Technol.*, 2022, doi: 10.1109/ODICON54453.2022.10010271.
[23] T. Sutikno, A. S. Samosir, dan R. A. Aprilianto, "Advanced DC – DC converter topologies for solar energy harvesting applications : a review," *Oxford Univ. Press behalf Natl. Inst. Clean-and-Low-Carbon Energ*, vol. 7, no. 3, hal. 555–570, 2023.
[24] A. Raj dan R. P. Praveen, "Highly efficient DC-DC boost converter implemented with improved MPPT algorithm for utility level photovoltaic applications," *Ain Shams Eng. J.*, vol. 13, no. 3, hal. 101617, 2022, doi: 10.1016/j.asej.2021.10.012.
[25] R. Dufo-l, "applied sciences Comparison of Lead-Acid and Li-Ion Batteries Lifetime Prediction Models in Stand-Alone Photovoltaic Systems," *Appl. Sci.*, vol. 11, no. 1099, 2021, doi: https:// doi.org/10.3390/app11031099.
[26] S. Mirjalili, S. M. Mirjalili, A. Lewis, C. Technology, dan S. Beheshti, "Grey Wolf Optimizer 1 1," *Adv. Eng. Softw.*, vol. 69, hal. 46–61, 2014, doi: 10.1016/j.advengsoft.2013.12.007.
[27] A. Seyyedabbasi dan F. Kiani, "Sand Cat swarm optimization : a nature - inspired algorithm to solve global optimization problems," *Eng. Comput.*, vol. 39, no. 4, hal. 2627–2651, 2023, doi: 10.1007/s00366-022-01604-x.
[28] F. MiarNaeimi, G. Azizyan, dan M. Rashk, "Horse herd optimization algorithm: A nature-inspired algorithm for high-dimensional optimization problems," *Knowledge-Based Syst.*, vol. 213, 2021, doi: https://doi.org/10.1016/j.knosys.2020.106711.
[29] I. Setyawan, R. M. Ariefianto, R. N. Hasanah, dan H. Suyono, "Improved MPPT Based on Flying Squirrel Search Optimization Using SEPIC for PV Systems," *Int. Conf. Power Eng. Appl.*, hal. 85–90, 2024, doi: 10.1109/ICPEA60617.2024.10498937.
[30] M. S. Braik, "Chameleon Swarm Algorithm: A bio-inspired optimizer for solving engineering design problems," *Expert Syst. Appl.*, vol. 174, 2021, doi: https://doi.org/10.1016/j.eswa.2021.114685.